Laser flash photolysis study of the photoinduced oxidation of 4-(dimethylamino)benzonitrile (DMABN)

Frank Leresche,[†, ‡, §] *Lucie Ludvíková,*[⊥] *Dominik Heger,*[⊥, *] *Petr Klán,*[⊥] *Urs von Gunten* [†, ‡] *and Silvio Canonica*[†, *]

[†]Eawag, Swiss Federal Institute of Aquatic Science and Technology, Überlandstrasse 133, CH-8600 Dübendorf, Switzerland

[‡]School of Architecture, Civil and Environmental Engineering (ENAC), Ecole Polytechnique Fédérale de Lausanne (EPFL), CH-1015 Lausanne, Switzerland

[⊥]Department of Chemistry and RECETOX, Faculty of Science, Masaryk University, Kamenice 5, 62500 Brno, Czech Republic

[§]Present address: Department of Civil, Environmental and Architectural Engineering, University of Colorado, Boulder, CO 80309, USA

Footnotes

* Corresponding Authors:

SC: Telephone: +41-58-765-5453. E-mail: silvio.canonica@eawag.ch.

DH: Telephone: +420 54949 3322. E-mail: hegerd@chemi.muni.cz.

Electronic Supplementary Information (ESI) comprising further experimental details and results as well as kinetic models and simulations descriptions is available.

Leresche, F., Ludvíková, L., Heger, D., Klán, P., von Gunten, U., & Canonica, S. (2019). Laser flash photolysis study of the photoinduced oxidation of 4-(dimethylamino)benzonitrile (DMABN). Photochemical and Photobiological Sciences, 18(2), 534-545. https://doi.org/10.1039/C8PP00519B

Abstract

Aromatic amines are aquatic contaminants for which phototransformation in surface waters can be induced by excited triplet states of dissolved organic matter (^{3}DOM*). The first reaction step is assumed to consist of a one-electron oxidation process of the amine to produce its radical cation. In this paper, we present laser flash photolysis investigations aimed at characterizing the photoinduced, aqueous phase one-electron oxidation of 4-(dimethylamino)benzonitrile (DMABN) as a representative of this contaminant class. The production of the radical cation of DMABN ($DMABN^{\bullet+}$) after direct photoexcitation of DMABN at 266 nm was confirmed in accord with previous experimental results. Moreover, $DMABN^{\bullet+}$ was shown to be produced from the reactions of several excited triplet photosensitizers (carbonyl compounds) with DMABN. Second-order rate constants for the quenching of the excited triplet states by DMABN were determined to fall in the range of $3 \times 10^7 – 5 \times 10^9$ M^{-1} s^{-1}, and their variation was interpreted in terms of electron transfer theory using a Rehm-Weller relationship. The decay kinetics of $DMABN^{\bullet+}$ in the presence of oxygen was dominated by a second-order component attributed to its reaction with the superoxide radical anion ($O_2^{\bullet-}$). The first-order rate constant for the transformation of $DMABN^{\bullet+}$ leading to photodegradation of DMABN was estimated not to exceed $\approx 5 \times 10^3$ s^{-1}.

1. Introduction

Aromatic amines constitute an important class of organic contaminants present in wastewaters and natural waters.[1-4] One of the major pathways contributing to their abatement in the aquatic environment is phototransformation induced by sunlight.[5-9] Besides direct phototransformation following absorption of sunlight by the contaminant, aromatic amines are subject to transformation photosensitized by dissolved organic matter (DOM). The latter is a complex mixture of cross-linked organic compounds derived from the degradation of higher plants or from microbial metabolic activity and ubiquitously present in natural waters.[10-13] Upon photoirradiation, the chromophoric components of DOM are promoted to their excited singlet states and subsequently excited triplet states (^{3}DOM*), which are likely to be the key reactive intermediates in the photosensitized transformation of aromatic amines in surface waters.[8, 14, 15] The initial reaction step in the photosensitized transformation is assumed to be an electron transfer from an aromatic amine to ^{3}DOM*.[16] This can be inferred from the abundant studies on the photoreduction of excited triplet carbonyls by amines,[17] arguments on the energetics of the redox reactions between substituted anilines and excited triplet states of aromatic ketones in aqueous solution,[14] and recent results on the quenching of the excited triplet state of methylene blue by substituted anilines.[15] Formation of a radical cation of the aromatic amine, a primary product of such an electron transfer reaction, is expected.

Studies performed during the last decade in our research group have revealed another important effect of DOM on the photosensitized transformation of anilines, which consists in reducing the rates of transformation. Reduction of transformation intermediates of the anilines by electron-donating (also called antioxidant) moieties of the DOM leading to reformation of the parent

compound was hypothesized to cause such an inhibition of transformation. Various pieces of evidence have been presented to support this hypothesis.[7, 14, 18-20]

The effects of DOM on the overall phototransformation rates of substituted anilines are now fairly well understood. However, very little is known about the nature and fate of the intermediates produced after the first oxidation step. The main goal of the present study is to characterize the kinetics of such intermediates derived from a model aniline in aqueous solutions. We selected 4-(dimethylamino)benzonitrile (DMABN, see Chart 1; DMABN can be named alternatively *N*,*N*-dimethyl-4-cyanoaniline[20]) for various reasons. Firstly, DMABN was used in a preceding steady-state photolysis kinetic study as a model compound to assess photosensitized transformation rates of aromatic amines and analogous compounds that undergo DOM-induced inhibition of oxidation in surface waters.[20] Secondly, the results of that study showed that the DOM-photosensitized transformation of DMABN very likely proceeds by direct reaction between DMABN and ^{3}DOM*, whereby singlet oxygen plays a negligible role. Thirdly, the two methyl substituents on the aniline group of DMABN make its radical cation (DMABN$^{\bullet+}$, see Chart 1) more resistant to deprotonation than the radical cations of anilines bearing no or only one substituent on the aniline group. Therefore, the relative stability of DMABN$^{\bullet+}$ is expected to provide favorable conditions for its direct observation in time-resolved experiments.

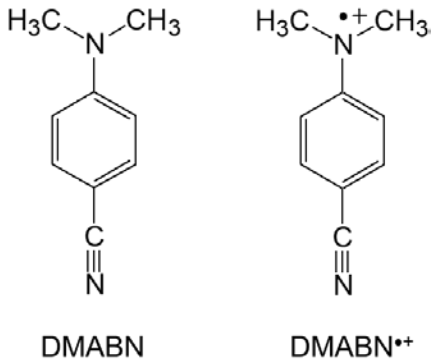

Chart 1. Structure of 4-(dimethylamino)benzonitrile (DMABN) and its radical cation (DMABN$^{\bullet+}$).

DMABN is the archetypal representative of aromatic compounds bearing both an electron-donating and an electron-accepting groups and exhibiting a dual fluorescence as well as excited-state charge separation in solutions.[21, 22] The excited singlet state characteristics and dynamics of such compounds, in particular DMABN, have been a hot research topic in ultrafast spectroscopy for a few decades.[21, 23-26] Nevertheless, information about the photophysics and photochemistry of DMABN on a microsecond or longer timescale is limited. The transient absorption spectrum observed on the microsecond scale after laser flash photolysis (LFP) of an aqueous solution of DMABN was interpreted as the superposition of various species:[27] these include the excited triplet state of DMABN (^{3}DMABN*, absorption maximum centered at 400 nm and a secondary broad band with a maximum at ≈600 nm[27]), the hydrated electron (e_{aq}^-, very broad absorption centered at ≈720 nm), and DMABN$^{\bullet+}$ (absorption maximum at ≈500 nm). While ^{3}DMABN* is formed through intersystem crossing from the lowest excited singlet state of DMABN (^{1}DMABN*, see Equation 1) with substantial quantum yields (a value of 0.55 was determined for an ethanol solution[27]), e_{aq}^- and DMABN$^{\bullet+}$ were formed through photoionization of DMABN (Equation 2). The photoionization of DMABN was found to be an excitation wavelength-dependent process mainly occurring at irradiation wavelengths of <280 nm. This indicated that photoionization did not involve ^{1}DMABN* but some higher excited states of DMABN.[27-29]

$$\text{DMABN} + h\nu \rightarrow {}^1\text{DMABN}^* \rightarrow {}^3\text{DMABN}^* \quad (1)$$

$$\text{DMABN} + h\nu \rightarrow \text{DMABN}^{\bullet+} + e_{aq}^- \quad (2)$$

The formation of DMABN$^{\bullet+}$ was implicitly assumed, but not directly observed, in a study on the reduction of excited triplet methylene blue by several aromatic amines.[30] DMABN$^{\bullet+}$ is believed to be the main species formed in natural waters upon oxidation of DMABN by ^{3}DOM*.[20]

The present study focuses on $DMABN^{\bullet+}$ formation and the description of its kinetics measured by LFP in aqueous solution. To form $DMABN^{\bullet+}$, direct photoexcitation and photosensitized oxidation of DMABN were employed. Simulations of the decay kinetics of $DMABN^{\bullet+}$ based on systems of reaction equations were also performed to evaluate its main reaction pathways. The results of these simulations were validated by comparison with experimental data.

2. Experimental section

2.1. Chemicals and solutions

All chemicals were commercially available and used as received. A complete list of chemicals is given in the Electronic Supplementary Information (ESI), Text S1. Water used for all experiments was obtained from an Aqua Osmotic 02A purification system. All sample solutions, made by diluting stock solutions of the reagents, were buffered using 2×10^{-3} M phosphate (total concentration) at pH 8.0, except when otherwise mentioned. Stock solutions were made in water except for the photosensitizers 3-methoxyacetophenone, 1-naphthaldehyde, 2-acetonaphthone and 1-acetonaphthone, for which acetonitrile (MeCN) was used as a cosolvent due to the limited solubility of these compounds in water. The concentration of MeCN in the sample solutions did not exceed 10% (v/v).

2.2. Laser flash photolysis (LFP) apparatus

Nanosecond LFP experiments were conducted using a 4 × 1 × 1 cm quartz cuvette containing the sample solution and laser pulses of the second, third or fourth harmonic frequency from a Nd:YAG laser (EKSPLA, model SL334). The LFP setup was operated in a perpendicular arrangement of the pump and probe beams. The laser pulses (pulse energies of 190–210 mJ at λ = 532 nm, 150–180

mJ at λ = 355 nm, and 70–90 mJ at λ = 266 nm; duration ≤170 ps) were dispersed on the 4-cm side of the cell using a cylindrical concave lens. Transient absorption spectra were recorded using an ICCD camera (Andor iStar, model DH740i-18U-03) with an overpulsed xenon arc lamp as a source of the probe light. Cut-off filters (480, 400, 380, 320 or 305 nm) were applied routinely to prevent the samples from unnecessary irradiation from the xenon lamp. The filtered light of the xenon lamp did not create transient spectra. Kinetic traces were recorded using the software TekScope on a Tektronix digital phosphor oscilloscope (model DPO7104C) at a single wavelength in the range of 400–670 nm (see ESI, Table S1 for the detection wavelength used in the measurement of each particular transient) with a monochromator using a Hamamatsu photomultiplier tube R928. Absorbance values of the sample solutions were usually adjusted to 0.5–0.8 (for a 1-cm optical path length) at the excitation wavelength. Samples were naturally aerated or degassed by applying three freeze-pump-thaw cycles under reduced pressure (8 Pa) or purged with a gentle stream of oxygen or N_2O for 15 minutes prior to measurements. For the determination of second-order quenching rate constants, nominal equilibrium concentration of dissolved gases for an ambient temperature of 21 °C and atmospheric pressure of 99 kPa were assumed. These correspond to 2.80×10^{-4} M and 1.33×10^{-3} M for dissolved oxygen in aerated and O_2-purged solution, respectively, and to 2.7×10^{-2} M for dissolved N_2O. Absorption spectra of the sample solutions were measured regularly between laser flashes to test for possible photodegradation of the solution components using the later described diode-array spectrophotometer. Experiments were conducted in an air-conditioned room at the temperature of 21±1 °C.

2.3 Kinetic analyses

The kinetic traces were generally fitted by single or multiple exponential decay functions using the software Flash Fit v. 0.11. In the case of second-order kinetics, the corresponding differential equations were solved using the software Matlab with the Levenberg-Marquard minimization algorithm or, alternatively, the software Kintecus© and applying the systems of equations and corresponding rate constants described in the ESI, Texts S2 and S3 and Tables S2 and S3. The observed rate constants, determined from single-exponential fitting of experimental data, are denoted in this paper with an additional superscript "obs", while the second-order rate constants obtained from fitting of experimental data or from observed first-order rate constants are denoted with an additional superscript "exp". The uncertainties of the rate constants given in the tables are expressed as 95% confidence intervals and were calculated using the values of at least three independent measurements.

2.4. Analytical instrumentation

Absorption spectra in the ultraviolet (UV) and visible (Vis) range were measured on an Agilent Cary 100 UV-Vis or an Agilent 8654 diode-array spectrophotometer. A BNC pHTestr 10 pH meter equipped with a calibrated glass electrode or an equivalent Eutech Instruments pH600 was used to measure the pH.

2.5 Kinetic models and simulations

The software Kintecus© was employed to simulate the buildup and decay kinetics of $DMABN^{\bullet+}$ and various relevant species occurring in DMABN-containing solutions after the short laser flash excitation.[31] Briefly, this software solves the system of differential equations derived from the chemical reaction equations for the system under study (i.e., the kinetic model), using a set of known reaction rate constants and initial concentrations of the species involved. The output

comprises the time course of the concentrations of each considered species. The systems of reaction equations and corresponding rate constants used in the present study are described in the ESI, Texts S2 and S3 and Tables S2 and S3.

3. Results and discussion

3.1. Direct excitation of 4-(dimethylamino)benzonitrile (DMABN)

Direct excitation of DMABN using laser pulses of 266 nm wavelength resulted in transient absorption spectra that are represented in Figure 1. A short-lived transient with a broad absorption band at 600–700 nm is evident at 5–60 ns delay times after excitation in aerated and oxygen-purged solutions (Figures 1A and 1B), while it is less apparent in an N_2O-purged solution (Figure 1C). This transient can be assigned to e_{aq}^-, which is known to react with dissolved oxygen and N_2O at diffusion-controlled rates.[29] The quenching of e_{aq}^- is more efficient in N_2O- than in O_2-purged solution because of the higher saturation concentration of N_2O compared to O_2 (*vide infra*). After the decay of e_{aq}^-, two broad bands are apparent at all measured conditions. The first of these bands has an absorption maximum at $\lambda \approx 400$ nm and its absorbance is strongly reduced 800 ns after the excitation, while the second band has an absorption maximum at $\lambda \approx 500$ nm and is especially discernible at long delay times (up to 5 μs) after the laser pulse. These species can be attributed to the excited triplet state of DMABN (^{3}DMABN*) and to the radical cation of DMABN (DMABN$^{\bullet+}$), respectively.[27] The kinetics of the three key species, namely e_{aq}^-, ^{3}DMABN* and DMABN$^{\bullet+}$, are described in more detail below.

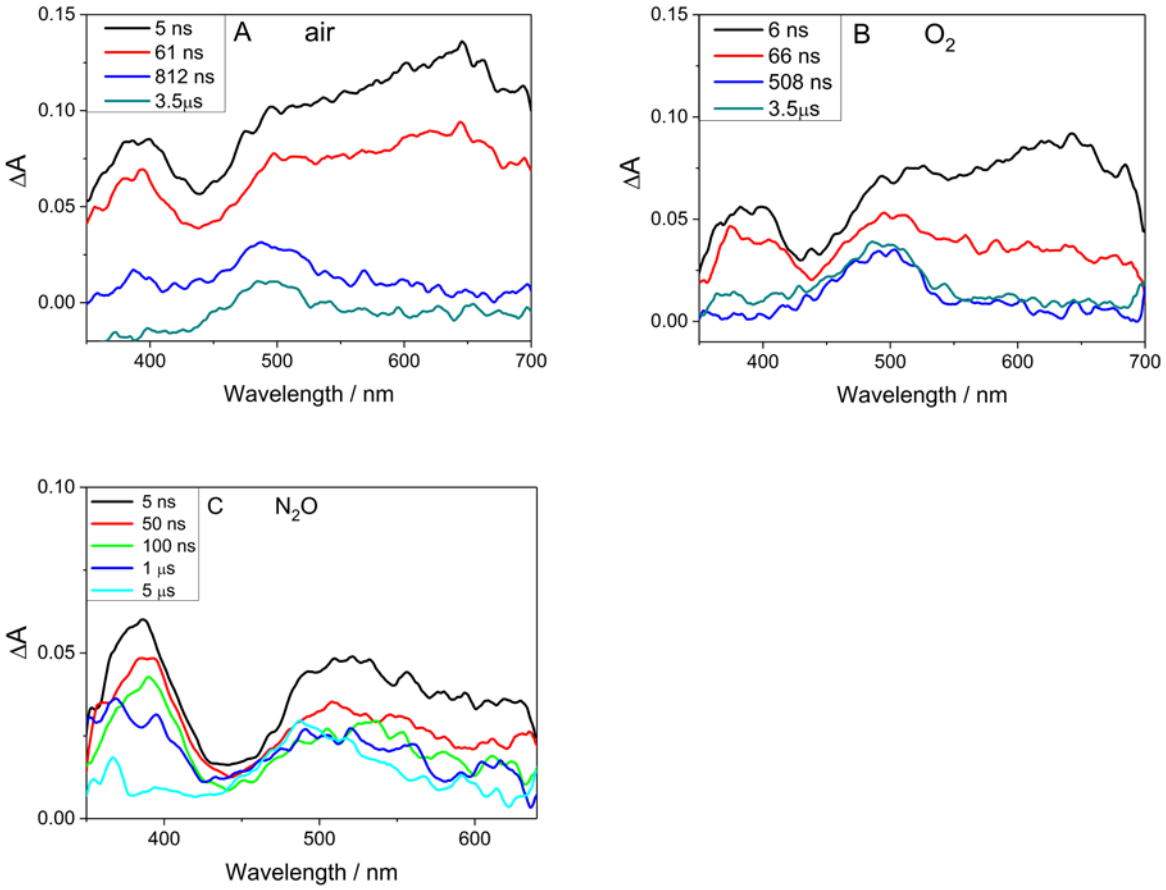

Figure 1. Transient absorption spectra obtained upon 266 nm laser flash photolysis of (A) DMABN (83 µM) in aerated solution, (B) DMABN (83 µM) in oxygen-purged solution, and (C) DMABN (133 µM) in N_2O-purged solution. The spectra were recorded in the time range of 5 ns to 5 µs after the laser pulse (see legend) using a 5-ns integration window, and data were smoothed by adjacent averaging over 20 data points (≈10 nm). All measurements were performed in pH 8.0 phosphate-buffered aqueous solutions.

3.1.1. Excited triplet state of DMABN (^{3}DMABN*)

The observed decay kinetics of ^{3}DMABN*, measured at 400 nm, was first order except for degassed solution and exhibited varying decay rate constants (see Table 1) depending on the

concentration of dissolved gases. In degassed solution, the first-order deactivation rate constant of ^{3}DMABN*, corresponding to the rate constant of the spontaneous decay of the triplet state, was determined to be $(3.92 \pm 0.12) \times 10^4$ s^{-1} by fitting the measured data with a kinetic model that included a second-order kinetic component to consider triplet–triplet annihilation (see ESI, Text S4). The determined decay rate constants in the presence of dissolved O_2 or N_2O were at least an order of magnitude higher than this value, and second-order rate constants for the quenching of ^{3}DMABN* by these two dissolved gases were obtained as given in Table 1. The deactivation of ^{3}DMABN* in the presence or absence of oxygen can be rationalized in terms of the processes described by Equations 3–9, whereby unimolecular deactivation (including contributions by the solvent, Equations 3–5) and triplet–triplet annihilation are dominant in degassed solution, while quenching by oxygen (Equations 7–9) is largely prevalent in aerated or oxygen-purged solution. A distinction of the processes within the groups of equations 3–5 and 7–9 is not possible in the frame of this study. However, we propose that the processes of reactive deactivation (Equation 5) and reactive quenching by oxygen (Equation 9) should have minor importance in view of the small quantum yield (1.3×10^{-3}) observed for the direct phototransformation of DMABN under steady-state irradiation in aerated solution.[20]

^{3}DMABN* $\rightarrow$ DMABN + $h\nu$ (phosphorescence) (3)

^{3}DMABN* $\rightarrow$ DMABN (non-radiative decay) (4)

^{3}DMABN* $\rightarrow$ Products (reactive deactivation) (5)

^{3}DMABN* + ^{3}DMABN* $\rightarrow$ ^{1}DMABN* +DMABN

(triplet–triplet annihilation) (6)

^{3}DMABN* +O_2 $\rightarrow$ DMABN +$^1O_2$ (energy transfer) (7)

$^3DMABN^* + O_2 \rightarrow DMABN + O_2$ (excitation energy loss) (8)

$^3DMABN^* + O_2 \rightarrow Products$ (reactive quenching) (9)

N_2O, used to scavenge e^-_{aq} (see the next sub-section) and not known as an excited triplet state quencher, also contributed to the quenching of $^3DMABN^*$ (described by Equation 10), although at a much lower rate than O_2.

$^3DMABN^* + N_2O \rightarrow DMABN + N_2O$ (excitation energy loss) (10)

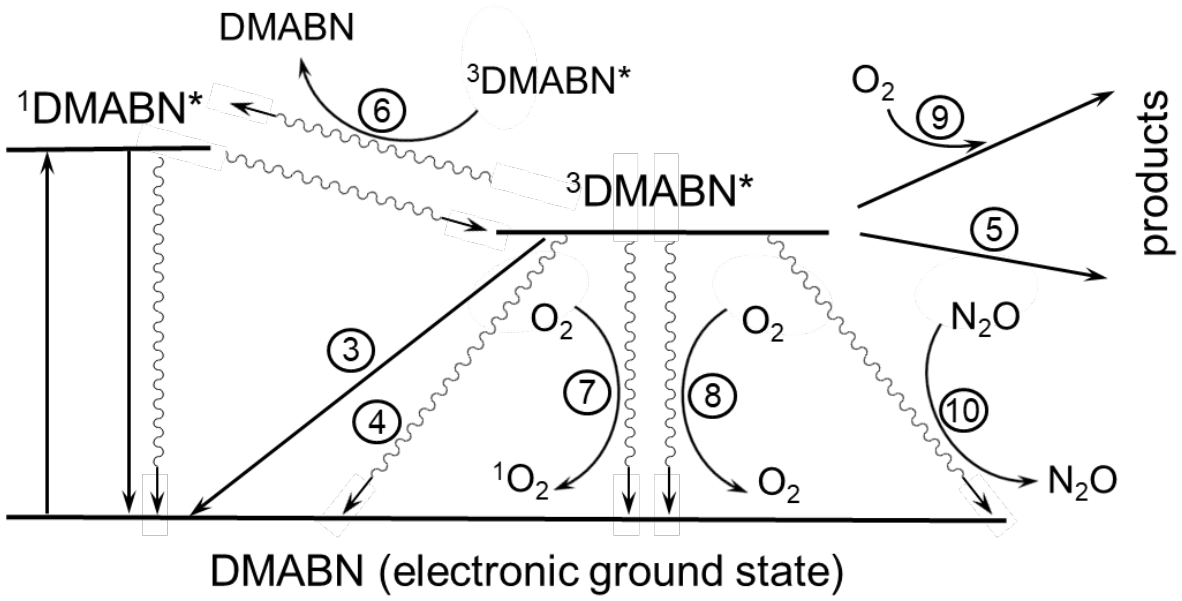

Chart 2. Relevant processes involving the excited triplet state of DMABN (^{3}DMABN*). Numbers correspond to the reaction equations listed in the text.

Table 1. Kinetic parameters determined for the deactivation of the main transient species formed during 266 nm laser flash photolysis of aqueous DMABN at pH 8.0 in the presence of various dissolved gases.

Transient species →	**^{3}DMABN***		e^-_{aq}		**DMABN$^{\bullet+}$**	
↓Dissolved gases	$k^{d,obs}_{^3DMABN^*}$ [a] / 10^6 s^{-1}	$k^{q,exp}_{^3DMABN^*,X}$ [b] / 10^9 M^{-1} s^{-1}	$k^{d,obs}_{e^-_{aq}}$ [c] / 10^7 s^{-1}	$k^{q,exp}_{e^-_{aq},X}$ [b] / 10^{10} M^{-1} s^{-1}	$k^{q,exp}_{DMABN^{\cdot+},O_2^{\cdot-}}$ [d] / 10^9 M^{-1} s^{-1}	$k^{d,obs}_{DMABN^{\cdot+}}$ / 10^4 s^{-1}
O_2 (1.33 mM)	5.0 ± 0.2	3.7	1.7 ± 0.1	1.3	9.4 ± 0.2	n.a. [e]
O_2 (0.28 mM)	1.70 ± 0.02	5.9	0.70 ± 0.06	2.5	8.1 ± 0.5	n.a.
N_2O (0.027 M)	0.647 ± 0.002	0.024	> 20 [f]	> 0.74 [f]	n.a.	1.24 ± 0.07 [g]
none (degassed)	0.039 ± 0.001 [h]	0.59 ± 0.02 [i]	n.a.	n.a.	n.a.	0.48 ± 0.12 [h]

Notes: [a] Observed first-order decay rate constants obtained by single-exponential fitting of the kinetic traces at λ_{obs} = 400 nm, unless where noted; [b] Second-order quenching rate constants calculated by dividing the difference of the observed first-order decay rate constants in the presence and absence of dissolved gas by the nominal gas concentration; [c] Observed first-order decay rate constants obtained by single-exponential fitting of the kinetic traces at λ_{obs} = 600 nm; [d] Second-order decay rate constant obtained from mixed first- and second-order fitting from the kinetic traces at λ_{obs} = 500 nm; [e] n.a.: not applicable; [f] Estimated as described in the text; [g] Observed first-order decay rate constant obtained by single-exponential fitting of the kinetic traces at λ_{obs} = 500 nm; [h] From ESI, Table S5, see text and ESI, Text S4 for the methods used for its determination; [i] Second-order rate constant for triplet-triplet annihilation from ESI, Table S5, see text and ESI, Text S4 for the methods used for its determination.

3.1.2. Hydrated electron (e_{aq}^-)

Upon LFP of DMABN in oxygenated aqueous solutions, the absorption corresponding to e_{aq}^- decayed by first-order kinetics with determined rate constants as given in Table 1. The derived second-order rate constants for the quenching of e_{aq}^- by O_2 (Table 1) are in good agreement with the literature value ($1.9 \times 10^{10}\ M^{-1}\ s^{-1}$) for the reaction of e_{aq}^- with oxygen to yield the superoxide radical anion ($O_2^{\bullet-}$, Equation 11).[29]

$$e_{aq}^- + O_2 \rightarrow O_2^{\bullet-} \qquad (11)$$

In degassed solution, the decay of e_{aq}^- was assumed to be dominated by its reaction with DMABN, and the aforementioned fitting procedure (ESI, Text S4) yielded a second-order rate constant value of $1.05 \times 10^{10}\ M^{-1}\ s^{-1}$ (ESI, Table S6). This value, which is close to the diffusion-controlled limit, is similar to the ones observed for the reaction of e_{aq}^- with other analogous compounds, such as benzonitrile ($1.9 \times 10^{10}\ M^{-1}\ s^{-1}$) and *p*-methylbenzonitrile ($1.4 \times 10^{10}\ M^{-1}\ s^{-1}$).[29] Other reactions of e_{aq}^- with buffer solution components (H^+, OH^-, H_2O, Na^+, $H_2PO_4^-$ and HPO_4^{2-}), with e_{aq}^- itself, and with $DMABN^{\bullet+}$ were estimated to be negligible.

In N_2O-purged solution, the signal corresponding to e_{aq}^- was not clearly detected even on a nanosecond time scale (see Figure 1C) due to fast scavenging by N_2O, which is known to lead to the formation of the hydroxyl radical and elementary nitrogen (Equation 12).[32, 33] Considering that 5 ns after the laser pulse < 37% of the absorbance signal at 600 nm is present if compared with an aerated solution (Figure 1), the second-order rate constant for the reaction of e_{aq}^- with N_2O

(Equation 12) can be estimated as >7.4×10^9 M^{-1} s^{-1}, which agrees well with the selected value of 9.1×10^9 M^{-1} s^{-1} reported in the literature.[29]

$$e^-_{aq} + N_2O + H_2O \rightarrow N_2 + {}^{\bullet}OH + OH^- \quad (12)$$

The very reactive hydroxyl radical, formed according to Equation 12, is expected to be completely scavenged by DMABN leading to the formation of intermediate products. These products are assumed not to be observable in the visible wavelength range and not to significantly interact with the other relevant transient species under the present experimental conditions.

3.1.3. Radical cation of DMABN (DMABN$^{\bullet+}$)

The decay of DMABN$^{\bullet+}$ in oxygen-containing solution was best fitted using a second-order kinetic component. In these solutions, the transient absorption traces measured at 500 nm were fitted using, in addition to the mentioned second-order component, two exponential functions with fixed decay constants to account for the observed first-order decay of ^{3}DMABN* and e^-_{aq}, which have a small but still significant absorption at the detection wavelength. An example of such a fitting is given in the ESI, Figure S2. The obtained second-order rate constants (Table 1) were assigned to the reaction of DMABN$^{\bullet+}$ (formed concomitantly with e^-_{aq} according to Equation 2) with $O_2^{\bullet-}$, which is the product of the reaction of e^-_{aq} with molecular oxygen (Equation 11), see Equation 13.

$$DMABN^{\bullet+} + O_2^{\bullet-} \rightarrow DMABN + O_2 \quad (13)$$

This assignment is based on the fact that, once formed, e^-_{aq} is scavenged by O_2 on the sub-microsecond time scale and, consequently, its reaction with DMABN$^{\bullet+}$ (Equation 14) does not

significantly contribute to the decay of the latter (see also kinetic simulations in the ESI, Figure S3).

$$DMABN^{\bullet+} + e^-_{aq} \rightarrow DMABN \quad (14)$$

A further postulated reaction is the transformation of $DMABN^{\bullet+}$ to yield the *N*-demethylated product 4-(methylamino)benzonitrile (MABN).[34] The proposed reaction sequence (Equation 15) considers an H-atom shift in $DMABN^{\bullet+}$ to produce an intermediate carbon-centered radical cation (abbreviated as $DMABNr^{\bullet+}$), which then deprotonates to give the radical $DMABNr^{\bullet}$.

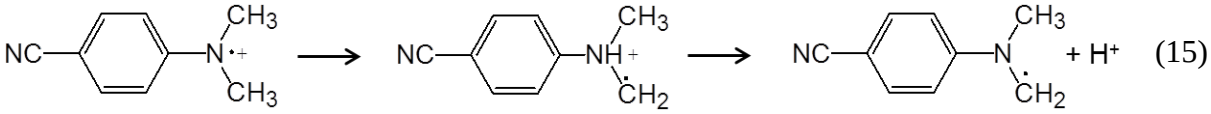

(15)

$DMABN^{\bullet+}$ $DMABNr^{\bullet+}$ $DMABNr^{\bullet}$

In degassed solution, application of the aforementioned fitting procedure that is described in the ESI, Text S5 yielded a first-order rate constant of $\approx 0.5 \times 10^4\ s^{-1}$ (see Table 1), which we assign to the transformation of $DMABN^{\bullet+}$ (Equation 15). In N_2O-purged solution, the decay of $DMABN^{\bullet+}$ fitted well first-order kinetics with a rate constant that was ≈2.6 times larger than the one determined in degassed solution (see Table 1). This first-order decay concurs with the expectation that $DMABN^{\bullet+}$ cannot undergo second-order reactions with e^-_{aq} (which is scavenged by N_2O) or $O_2^{\bullet-}$ (which cannot be formed under these solution conditions).

3.1.4. pH Effect

The decay kinetics of ^{3}DMABN* and DMABN$^{\bullet+}$ was studied in aerated and N_2O-purged solutions at various pH values, with the aim of getting additional information about the processes involved. The results of the fittings, performed as described in the previous sub-sections, are gathered in the ESI, Table S6. For ^{3}DMABN*, the deactivation rate constant in aerated solution was not significantly affected by pH in the range of 4.5–7.7 (average ± standard deviation: $(1.75 \pm 0.04) \times 10^6$ s^{-1}), while in N_2O-purged solution it was pH-dependent with an increase by a factor of ≈2 at pH 7.7 compared to the lower pH range. We tentatively attribute this increase related to the quenching of ^{3}DMABN* by N_2O to an effect of the used phosphate buffer, with HPO_4^{2-} being the dominant species at pH 7.7, while at the lower investigated pH values $H_2PO_4^-$ is predominant. For DMABN$^{\bullet+}$ in aerated solutions, the obtained second-order rate constant values were invariable in the pH range of 5.4–7.7 ($(7.7 \pm 0.4) \times 10^9$ M^{-1} s^{-1}), but the value at pH 4.5 was significantly lower ($(4.0 \pm 0.2) \times 10^9$ M^{-1} s^{-1}). This concurs with a major change in speciation of $O_2^{\bullet-}$, which is mainly protonated to its conjugated acid, the hydroperoxyl radical ($HO_2^{\bullet}$), at pH 4.4 (note: the pK_a of $HO_2^{\bullet}$ is 4.8).[35] The reduction in rate constant is plausible, because $HO_2^{\bullet}$ is a weaker electron donor than $O_2^{\bullet-}$. For DMABN$^{\bullet+}$ in N_2O-purged solutions, the obtained first-order rate constant values vary by only ±15% in the pH range of 4.5–7.7, which let us conclude that the transformation of DMABN$^{\bullet+}$ is not affected by protonation reactions in this pH range.

3.2. Photosensitized formation of DMABN$^{\bullet+}$

Several photosensitizers were used as a means to oxidize DMABN to DMABN$^{\bullet+}$. Upon excitation of a photosensitizer (Sens) its excited triplet state (^{3}Sens*) is formed through intersystem crossing from the excited singlet states (Equation 16). ^{3}Sens* can act in certain cases as a powerful oxidant. Especially aromatic ketones and quinones possess standard one-electron reduction potentials, $E_{\mathrm{red}}^{0*}\left({}^3\mathrm{Sens}^*/\mathrm{Sens}^{\bullet-}\right)$, that can be in the range of 1.8–2.4 V vs. standard hydrogen electrode (SHE) and are thus comparable to those of the strongest radical oxidants.[36, 37] The oxidation reaction of DMABN by ^{3}Sens* is expected to produce DMABN$^{\bullet+}$ as well as the radical anion of the photosensitizer (Sens$^{\bullet-}$) within the lifetime of ^{3}Sens* (Equation 17). Besides the unimolecular and bimolecular deactivation processes that were listed for ^{3}DMABN* (Equations 3–9), oxidizing ^{3}Sens* are expected to undergo the following additional reactions with DMABN: Excitation energy loss (Equation 18) and triplet–triplet energy transfer from ^{3}Sens* to DMABN (Equation 20). Both reactions 17 and 18 have been observed during the quenching of excited triplet methylene blue by DMABN in methanol solution with a ratio of 1:3 between electron transfer and physical quenching.[30] While we are not aware of any method that could be used to maximize the yield of DMABN$^{\bullet+}$ formation during quenching, the energy transfer reaction (Equation 19), and consequently the formation of ^{3}DMABN*, can be suppressed by choosing photosensitizers with a lower triplet energy than DMABN.

$$\mathrm{Sens} + h\nu \rightarrow {}^1\mathrm{Sens}^* \rightarrow {}^3\mathrm{Sens}^* \qquad (16)$$

$$^3\mathrm{Sens}^* + \mathrm{DMABN} \rightarrow \mathrm{Sens}^{\bullet-} + \mathrm{DMABN}^{\bullet+} \quad \text{(oxidative quenching)} \qquad (17)$$

$$^3\mathrm{Sens}^* + \mathrm{DMABN} \rightarrow \mathrm{Sens} + \mathrm{DMABN} \quad \text{(excitation energy loss)} \qquad (18)$$

$$^3\mathrm{Sens}^* + \mathrm{DMABN} \rightarrow \mathrm{Sens} + {}^3\mathrm{DMABN}^* \quad \text{(triplet–triplet energy transfer)} \qquad (19)$$

To avoid direct excitation of DMABN, the 355 nm and 532 nm excitation wavelengths of the laser were used to selectively produce ^{3}Sens*. The sensitizers were selected to significantly absorb light at one of these excitation wavelengths (see the electronic absorption spectra in the ESI, Figure S4) and to cover a range of one-electron reduction potentials that could be used to estimate the oxidation potential of DMABN in aqueous solution (presently unknown). Moreover, practical aspects, such as the aqueous solubility of the photosensitizers and the feasibility of their selective excitation were considered.

3.2.1. Transient absorption spectra

To disentangle the spectra of ^{3}Sens*, Sens$^{\bullet-}$ and DMABN$^{\bullet+}$ present after LFP of solutions containing a given photosensitizer and DMABN, and to select suitable observation wavelengths for the kinetic measurements, the following procedure was applied: (1) Generation of the ^{3}Sens* from a buffered solution of the photosensitizer alone; (2) generation of ^{3}Sens*, and subsequently Sens$^{\bullet-}$, from a buffered solution containing the photosensitizer and triethanolamine (TEA. Note: the radicals formed by the oxidation of TEA absorb outside of the considered spectral range[38]); (3) production of the three species, i.e., ^{3}Sens*, Sens$^{\bullet-}$ and DMABN$^{\bullet+}$, in a buffered solution of the photosensitizer and DMABN. Figure 2 shows an illustrative example of this procedure using 2-acetonaphthone (2-AN) as a model photosensitizer (for a collection of transient absorption spectra for the other photosensitizers, see the ESI, Texts S5–S9 and Figures S5–S9). The transient absorption spectrum of the excited triplet state of 2-AN (^{3}2-AN*) has a maximum at $\lambda \approx$440 nm (Figure 2A), while the spectrum of the radical anion of 2-AN (2AN$^{\bullet-}$) overlaps partly with that of ^{3}2-AN* but has its maximum absorption at $\lambda \approx$400 nm (Figure 2B). The transient absorption spectra shown in Figure 2C contain a dominating superposition of ^{3}2-AN* and 2-AN$^{\bullet-}$ at short

delay times (up to ≈500 ns) after the laser pulse, but at longer delay times a band centered at ≈500 nm clearly emerged. This was assigned to $DMABN^{\bullet+}$ based on its similarities to the spectra of $DMABN^{\bullet+}$ observed from direct photoexcitation of DMABN in this study (Figure 1) and in previous studies.[27, 39] Note that the presence of oxygen is beneficial to the observation of $DMABN^{\bullet+}$, because it accelerates the decay of $Sens^{\bullet-}$ (in this case $2\text{-}AN^{\bullet-}$) according to Equation 20, leaving $DMABN^{\bullet+}$ as the only absorbing species in the considered spectral range at long delay times.

$$Sens^{\bullet-} + O_2 \rightarrow Sens + O_2^{\bullet-} \qquad (20)$$

The transient absorption spectra shown in Figure 2 were utilized to evaluate the optimal observation wavelength to be used for the measurement of kinetic traces and the determination of decay rate constants of the various species. Figure 2D displays an example of a linear regression plot of deactivation rate constants of ^{3}2-AN* determined at various DMABN concentrations, which was used to determine the second-order rate constant for the quenching of ^{3}2-AN* by DMABN.

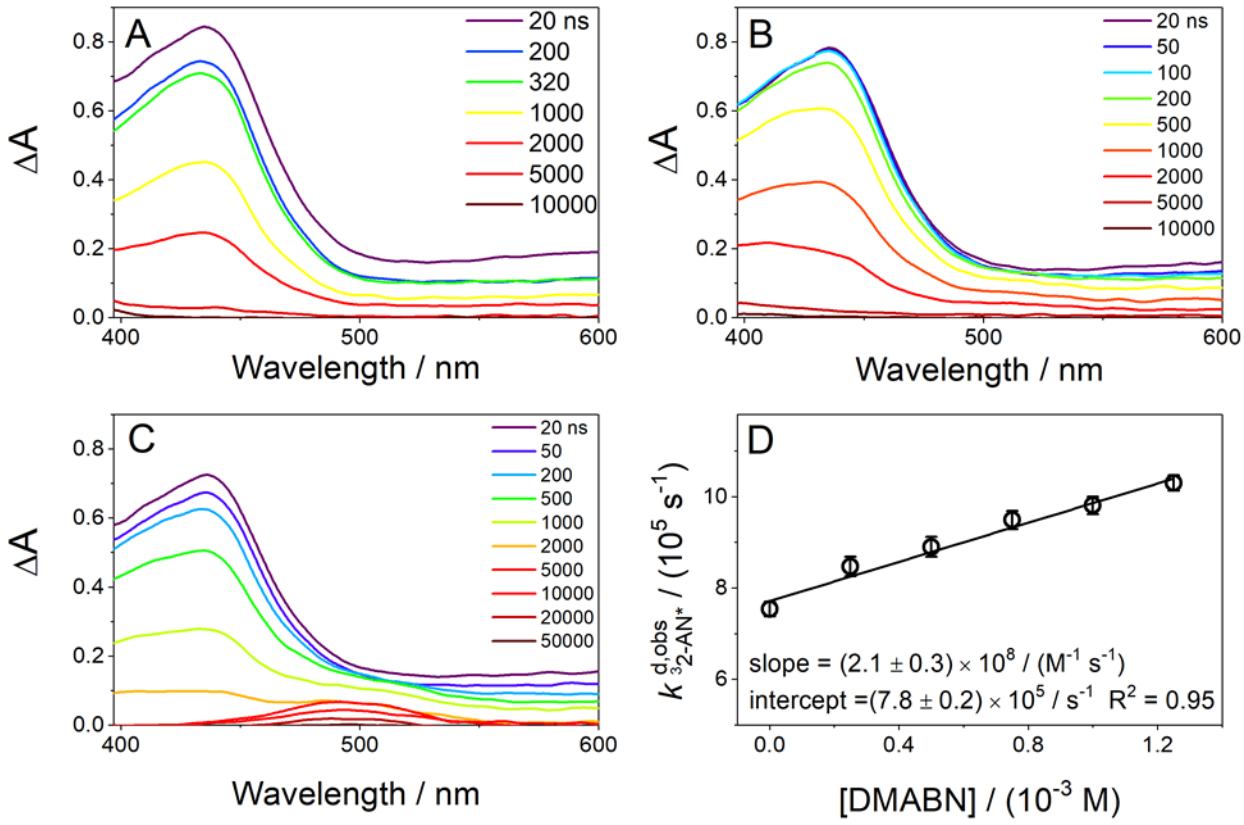

Figure 2. A–C: Transient absorption spectra following 355 nm laser pulse excitation of: (A) 2-Acetonaphthone (2-AN, 5×10^{-4} M); (B) 2-AN (5×10^{-4} M) and triethanolamine (TEA, 1×10^{-2} M); (C) 2-AN (5×10^{-4} M) and DMABN (5×10^{-4} M). Spectra were recorded in the time range from 20 ns to 50 μs after the laser pulse using a 5-ns integration window. Spectral data were smoothed by adjacent averaging over 20 data points (≈10 nm). All samples (pH 8.0) were made in aerated water containing 0.9% (v/v) MeCN. (D) A plot of the determined first-order decay rate constant of the triplet state of 2-AN (obtained at the observation wavelength of 520 nm) vs. the DMABN concentration. Error bars represent 95% confidence intervals from at least quadruplicate measurements.

3.2.2. Quenching of the excited triplet state of photosensitizers by DMABN

For photosensitizers having oxidizing excited triplet states, quenching rate constants can be used as an indicator of the efficacy in producing the oxidized substrate. To produce $DMABN^{\bullet+}$ at sufficiently high concentration for an accurate evaluation of its decay kinetics, high ^{3}Sens* second-order quenching rate constants are advantageous. Table 2 collects the second-order quenching rate constants obtained in this study for six photosensitizers exhibiting E_{red}^{0*} values in the range of 1.26–1.86 V vs. SHE. The corresponding linear regression plots are given in Figure 4D for 2-AN and in the ESI, Figure S9 for the other photosensitizers. The quenching rate constants vary over about two orders of magnitude and increase non-linearly with increasing E_{red}^{0*}. Literature values of the triplet state energies of the photosensitizers are also collected in Table 3 to evaluate the possibility of energy transfer as a side-reaction (Equation 20). Only 3-methoxyacetophenone (E_T = 3.14 eV)[40] has a higher triplet state energy than DMABN (2.81 eV)[27], but no evidence for the formation of ^{3}DMABN* could be found in the measured transient absorption spectra with this photosensitizer. For all other photosensitizers energy transfer can be excluded *a priori*.

Table 2. Ground-state reduction potentials (E^0_{red}), triplet-state reduction potentials (E^{0*}_{red}), triplet state energies (E_T) and determined second-order rate constants of triplet state quenching by DMABN ($k^{q,obs}_{^3Sens^*,DMABN}$) for the studied photosensitizers

Photosensitizer	E^0_{red} [a] / V vs. SHE	E^{0*}_{red} [a] / V vs. SHE	E_T [a] / eV	$k^{q,obs}_{^3Sens^*,DMABN}$ [b] / 10^9 M^{-1} s^{-1}
9,10-Anthraquinone-1,5-disulfonate	–0.5	1.86	2.36	5.02 ± 0.16
3-Methoxyacetophenone	–1.43 [c]	1.71 [c]	3.14 [c]	4.0 ± 0.2 [d]
Thionine	–0.25	1.45	1.70	4.6 ± 0.3
1-Naphthaldehyde [c]	–1.11	1.34	2.45	3.4 ± 0.3 [e]
2-Acetonaphthone [c]	–1.25	1.34	2.59	0.21 ± 0.03 [e]
1-Acetonaphthone [c]	–1.26	1.26	2.52	0.031 ± 0.017 [e]

Notes: [a]Standard one-electron reduction potentials of the photosensitizers in their electronic ground state (E^0_{red}) and excited triplet state (E^{0*}_{red}) as well as triplet state energies (E_T) obtained from Ref. 36 unless otherwise noted; [b]Measured in aerated aqueous solution at pH 8.0. Errors represent 95% confidence intervals obtained from the linear regression lines; [c]From Ref. 40; [d]Solutions containing 10% (v/v) MeCN; [e]Solutions containing ≈1% (v/v) MeCN.

In the following we analyze the rate constants for triplet state quenching by DMABN, k^q, in the frame of electron transfer theory, more precisely by using the Rehm-Weller relationship (Equation 21).[41-43]

$$k^{q} = \frac{k_d}{1 + \frac{k_d}{K_d Z}\left\{\exp\left[\left(\sqrt{\left(\frac{\Delta_r G_{et}^0}{2}\right)^2 + \left(\frac{\lambda}{4}\right)^2} + \left(\frac{\Delta_r G_{et}^0}{2}\right)\right) / RT\right] + \exp\left(\frac{\Delta_r G_{et}^0}{RT}\right)\right\}} \quad (21)$$

The parameters are defined as follows: k_d and k_{-d} are the rate constants for the formation and separation of the precursor complex, respectively, $K_d = k_d/k_{-d}$ is the equilibrium constant for the precursor complex formation, Z is the universal collision frequency factor, R is the universal gas constant, T is the absolute temperature, λ is the reorganization energy, and $\Delta_r G_{et}^0$ is the standard molar free energy change of the electron transfer reaction, i.e., the standard molar free energy difference between successor complex and precursor complex, which was approximated using Equation 22.

$$\Delta_r G_{et}^0 \cong F \times \left(E_{red}^0\left(\text{DMABN}^{\bullet+}/\text{DMABN}\right) - E_{red}^{0*}\left({}^3\text{Sens}^*/\text{Sens}^{\bullet-}\right)\right) \quad (22)$$

To fit the determined second-order rate constants for quenching of ^{3}Sens* by DMABN, Equation 22 was inserted in Equation 21, and $E_{red}^{0*}\left({}^3\text{Sens}^*/\text{Sens}^{\bullet-}\right)$ was used as the independent variable while $E_{red}^0\left(\text{DMABN}^{\bullet+}/\text{DMABN}\right)$ was a fitting parameter. A similar procedure as in Ref. 44 was applied, keeping the ratio $k_d/(K_d \times Z)$ fixed at 0.1. λ was used as an additional fitting parameter, while k_d was fixed at 5.0×10^9 M^{-1} s^{-1}. Fits to the Rehm-Weller model are represented in Figure 3, whereby fits with various fixed values of λ are also shown. The fit to the Rehm-Weller model with two fitting parameters gave values of 0 kJ mol^{-1} for λ and 1.32 ± 0.04 V vs. SHE for $E_{red}^0\left(\text{DMABN}^{\bullet+}/\text{DMABN}\right)$. Using a fixed value of λ = 20 kJ mol^{-1} (a value which was obtained for the quenching of the excited triplet state of methylene blue by a series of substituted anilines [15]) also yields a reasonably good fit with $E_{red}^0\left(\text{DMABN}^{\bullet+}/\text{DMABN}\right)$ = 1.28 ± 0.08 V vs. SHE

(used as the only fitting parameter). Both values are significantly higher (by 0.13 and 0.09 V, respectively) than a crude estimate of 1.19 V obtained by adding the difference between the oxidation potentials of 4-cyanoaniline (1.32 V)[45] and aniline (1.00 V)[45] to the oxidation potential of *N*,*N*-dimethylaniline (0.87 V),[46] all measured in aqueous solution. Note that a value of 1.11 V for $E^{0}_{\mathrm{red}}\left(\mathrm{DMABN}^{\bullet+}/\mathrm{DMABN}\right)$ was determined in MeCN solution,[47] which is even lower than the aforementioned crude estimate.

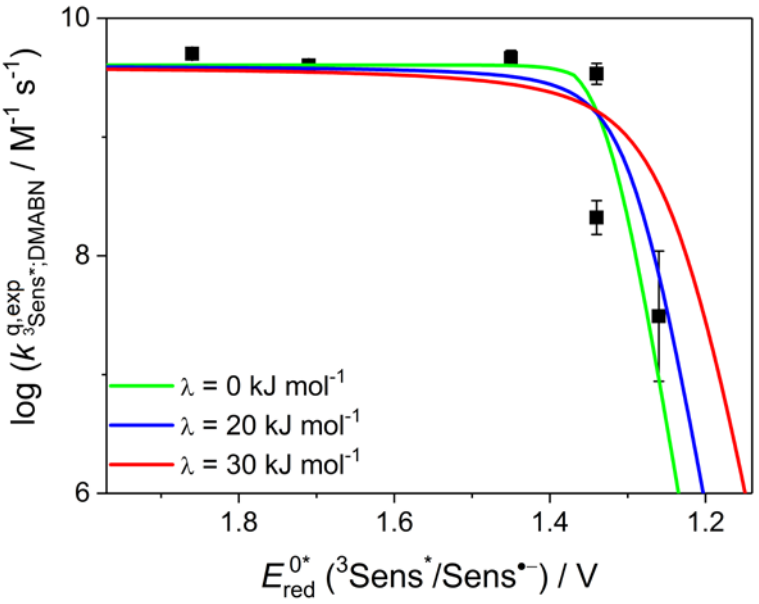

Figure 3. Determined second-order rate constants for the quenching of excited triplet states of photosensitizers by DMABN ($k^{\mathrm{q}}_{^3\mathrm{Sens}^*,\mathrm{DMABN}}$) (black squares) plotted on a logarithmic scale against $E^{0*}_{\mathrm{red}}\left(^3\mathrm{Sens}^*/\mathrm{Sens}^{\bullet-}\right)$, the one-electron reduction potential of the excited triplet states of the photosensitizers. The lines represent fits to the Rehm-Weller model with reorganization energy (λ) values as given in the legend. The fitting procedure is explained in the text. Error bars represent 95% confidence intervals obtained from plots of triplet state decay rate constants against DMABN concentration (see Figures 2D and S7).

3.2.3. Decay kinetics of $DMABN^{\bullet+}$

The $DMABN^{\bullet+}$ decay kinetics was studied at various "initial" $DMABN^{\bullet+}$ concentrations with the main aim of evaluating the relative importance of first- and second-order kinetic processes. A series of experiments was conducted at constant DMABN concentration (5×10^{-4} M) using 1-naphthaldehyde (1-NA) as the photosensitizer. Thereby, the "initial" concentration of ^{3}1-NA* (measured ≈10 ns after the laser pulse) was tuned by varying the concentration of 1-NA in the range of $5 \times 10^{-5} – 3 \times 10^{-4}$ M, and additionally by varying the laser pulse intensity using metal-grid filters (experiments conducted at [1-NA] = 5×10^{-5} M). The transient absorbance change data were first analyzed using conventional second-order kinetic plots as detailed in the ESI, Text 10, Figure S11 and Table S7. Especially at the high 1-NA concentrations, and consequently at the high "initial" ^{3}1-NA* and $DMABN^{\bullet+}$ concentrations, this simple kinetic analysis yielded consistent values for the second-order rate constant, which was assigned to the reaction of $DMABN^{\bullet+}$ with $O_2^{\bullet-}$ (Equation 13). With decreasing initial concentration of the considered transient species, deviation from the simple second-order kinetic model became increasingly apparent, which was interpreted as an increasing impact of the transformation of $DMABN^{\bullet+}$ (Equation 15) on its decay. Kinetic simulations, performed according to the details given in the ESI, Text S3 and Table S3 and displayed in Figure S12, supported this hypothesis. Moreover, these simulations revealed that the concentrations of $DMABN^{\bullet+}$ and $O_2^{\bullet-}$ at a given time point are generally different, meaning that the condition to apply the simple second-order kinetic model are not fulfilled. Therefore, a complete analysis in terms of differential equations representing the kinetic system is required for an adequate evaluation of the $DMABN^{\bullet+}$ decay data.

Data fitting was performed using Kintecus© and the kinetic model presented in the ESI, Text S3 and Table S3. For the fittings, the initial concentration of the excited triplet state of 1-NA, $[^3$1-NA*$]_0$, was estimated using the procedure described in the ESI, Table S7 and employed as a fixed parameter, while the molar absorption coefficient of $DMABN^{\bullet+}$, the second-order rate constant for the reaction between $DMABN^{\bullet+}$ and $O_2^{\bullet-}$, $k^{q,exp}_{DMABN^{\cdot+},O_2^{\cdot-}}$, and the first-order rate constant for the transformation of $DMABN^{\bullet+}$ (see Equation 15), $k^{d,obs}_{DMABN^{\cdot+}}$, were used as fitting parameters. Figure 4 shows that the fittings were able to accurately describe the experimental kinetic traces, however the obtained best-fit parameters varied depending on the estimated $[^3$1-NA*$]_0$ (see ESI, Table S8). With decreasing $[^3$1-NA*$]_0$ (from 63 to 1.9 μM), fitted $k^{q,exp}_{DMABN^{\cdot+},O_2^{\cdot-}}$ values steadily increased from 5.2×10^9 to 1.2×10^{10} M^{-1} s^{-1}, while the fitted values of the molar absorption coefficient of $DMABN^{\bullet+}$ increased from ≈2400 M^{-1} cm^{-1} to values in the rather narrow range of ≈3500 – 3800 M^{-1} cm^{-1} for $[^3$1-NA*$]_0 \leq 14$ μM. For the third fitting parameter, $k^{d,obs}_{DMABN^{\cdot+}}$, it was not possible to obtain a reliable estimate (the lower limit of 100 s^{-1} that was set as a constraint in the fitting procedure was attained for most decays). The only successful estimation, obtained for $[^3$1-NA*$]_0$ = 1.92 μM, yielded a value of $(1.2 \pm 0.5) \times 10^3$ s^{-1}, which is much lower than the estimate of $k^{d,obs}_{DMABN^{\cdot+}}$ obtained from direct photoexcitation experiments in degassed solution (see Table 1).

A preferred value of $k^{q,exp}_{DMABN^{\cdot+},O_2^{\cdot-}} = (5.2 \pm 0.4) \times 10^9$ M^{-1} s^{-1} (mean ± s. d.) was calculated by averaging the values obtained at the two highest $[^3$1-NA*$]_0$. This was done considering the fact that at these $[^3$1-NA*$]_0$ values the reaction between $DMABN^{\bullet+}$ and $O_2^{\bullet-}$ largely dominates the decay of $DMABN^{\bullet+}$, while at lower $[^3$1-NA*$]_0$ values the increasing importance of the first-order decay process of $DMABN^{\bullet+}$ is expected to bias the determination of $k^{q,exp}_{DMABN^{\cdot+},O_2^{\cdot-}}$. The preferred

value of $k^{q,exp}_{DMABN^{\cdot+},O_2^{\cdot-}}$ is significantly lower than the value obtained by the second-order fittings ((1.6 ± 0.1) ×10^{10} M^{-1} s^{-1}, see ESI, Text S10 and Table S7) and the values obtained from the direct photoexcitation experiments in the presence of air and oxygen ((8.1 ± 0.5) and (9.4 ± 0.2) ×10^9 M^{-1} s^{-1}, respectively, see Table 1). The difference to the latter values might be due to the different assumptions adopted when performing the various types of fittings. Using this value of 5.2 × 10^9 M^{-1} s^{-1} as fixed input parameter for $k^{q,exp}_{DMABN^{\cdot+},O_2^{\cdot-}}$, a two-parameters fitting of the $[^3$1-NA*$]_0$ = 1.92 μM data was performed, which yielded a value of (3.5 ± 1.4) × 10^3 s^{-1} for the first-order transformation of $DMABN^{\bullet+}$. This value is not far from (4.8 ± 1.2) × 10^3 s^{-1}, the value obtained from direct photoexcitation of DMABN in degassed solutions (see Table 1). To our knowledge, this represents the first estimation of a deprotonation rate constant for an *N*,*N*-dimethylaniline radical cation in aqueous solution. Previous studies on such radical cations performed using organic solvents and acetate as a proton acceptor[48, 49] support the assignment of this rate constant to a deprotonation reaction as illustrated by Equation 15.

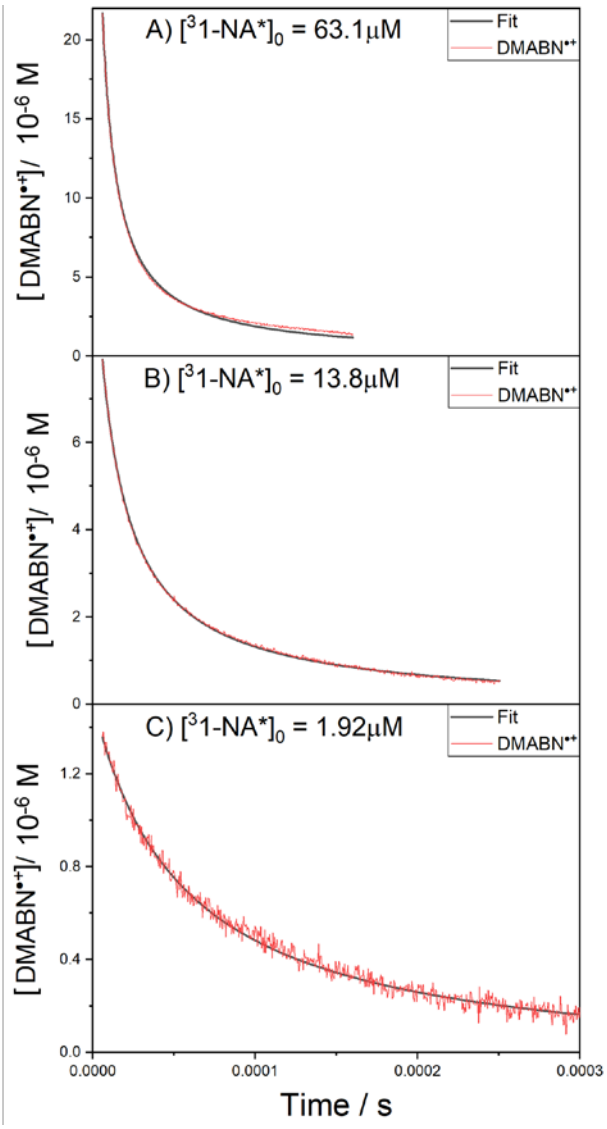

Figure 4. Decay traces of $DMABN^{\bullet+}$ (red lines, observation wavelength 500 nm) formed by laser flash excitation of 1-Naphthaldehyde (1-NA) at 355 nm. Experiments were performed with constant $[DMABN]_0 = 5 \times 10^{-4}$ M and various $[1\text{-NA}]_0$ and metal grid filters (see text). Black curves represent fits performed using Kintecus© as described in the text. Panels A–C contain decay traces measured at different initial concentrations of ^{3}1-NA*, $[^3\text{1-NA*}]_0$, estimated as given in the ESI, Table S7. The obtained fit parameters are collected in the ESI, Table S8.

4. Conclusions

This study focused on the formation and decay of the radical cation of DMABN, $DMABN^{\bullet+}$, which was produced in aqueous solution by laser flash excitation of either DMABN or a photosensitizer inducing the oxidation of DMABN. $DMABN^{\bullet+}$, with a maximum absorption at a wavelength of ≈500 nm, was the longest-lived transient intermediate observed in the visible spectral range, and was detected in a time delay range extending over several 100 μs. The photosensitized formation of $DMABN^{\bullet+}$ was found to be efficient using sensitizers with estimated triplet-state standard one-electron reduction potential of >≈1.34 V vs. SHE, and for these sensitizers a rate constant for the quenching of their excited triplet state by DMABN of $>3 \times 10^9$ M^{-1} s^{-1} was observed. On the nanosecond time scale, the primary by-products of $DMABN^{\bullet+}$ formed upon laser flash photolysis of DMABN and of a sensitizer (Sens) were the hydrated electron, e_{aq}^-, and the radical anion of the sensitizer, $Sens^{\bullet-}$, respectively. In aerated solution, these species reacted with molecular oxygen with half-lifetimes of ≈100 ns and ≈0.7 – 2 μs, respectively, to yield the superoxide radical anion ($O_2^{\bullet-}$, not monitored in this study). In oxygen-containing solution under the LFP conditions of this study, the deactivation of $DMABN^{\bullet+}$ appeared to be dominated by its reaction with $O_2^{\bullet-}$, leading to the reformation of DMABN. For steady-state irradiation conditions as typical for sunlit surface waters, where much lower concentrations of $O_2^{\bullet-}$ were detected (10^{-12}–10^{-9} M)[50], the reaction with $O_2^{\bullet-}$ should be negligible. From direct photoexcitation experiments performed in degassed solution as well as photosensitization experiments, the first-order transformation of $DMABN^{\bullet+}$, which was primarily assigned to its deprotonation, may be estimated to take place with rate constants not exceeding $\approx 5 \times 10^3$ s^{-1}. The reaction of $DMABN^{\bullet+}$ with dissolved organic matter, an important

natural water component, will be the subject of a follow-up study intended to assess the phototransformation rates of DMABN and analogous aquatic contaminants in surface waters.

Acknowledgements

The authors would like to thank Luboš Jílek for the technical support with the laser system. This work was supported by the Swiss National Science Foundation (Project No. 200021-140815). The RECETOX research infrastructure was supported by the projects of the Czech Ministry of Education (LO1214 and LM2011028).

Conflicts of interest

There are no conflicts to declare.

References

1. W. W. Stone, R. J. Gilliom and K. R. Ryberg, Pesticides in U.S. streams and rivers: occurrence and trends during 1992-2011, *Environ. Sci. Technol.*, 2014, **48**, 11025-11030.
2. C. Moschet, I. Wittmer, J. Simovic, M. Junghans, A. Piazzoli, H. Singer, C. Stamm, C. Leu and J. Hollender, How a complete pesticide screening changes the assessment of surface water quality, *Environ. Sci. Technol.*, 2014, **48**, 5423-5432.
3. T. A. Ternes, Occurrence of drugs in German sewage treatment plants and rivers, *Water Res.*, 1998, **32**, 3245-3260.
4. X. S. Miao, F. Bishay, M. Chen and C. D. Metcalfe, Occurrence of antimicrobials in the final effluents of wastewater treatment plants in Canada, *Environ. Sci. Technol.*, 2004, **38**, 3533-3541.
5. K. Othmen and P. Boule, Photochemical behaviour of dichloroanilines in water and formation of aminochlorophenoxazones, *J. Photochem. Photobiol. A- Chem.*, 1999, **121**, 161-167.
6. D. Vialaton, J. F. Pilichowski, D. Baglio, A. Paya-Perez, B. Larsen and C. Richard, Phototransformation of propiconazole in aqueous media, *J. Agr. Food Chem.*, 2001, **49**, 5377-5382.

7. S. Canonica and H. U. Laubscher, Inhibitory effect of dissolved organic matter on triplet-induced oxidation of aquatic contaminants, *Photochem. Photobiol. Sci.*, 2008, **7**, 547-551.

8. A. L. Boreen, W. A. Arnold and K. McNeill, Triplet-sensitized photodegradation of sulfa drugs containing six-membered heterocyclic groups: identification of an SO_2 extrusion photoproduct, *Environ. Sci. Technol.*, 2005, **39**, 3630-3638.

9. J. J. Guerard, P. L. Miller, T. D. Trouts and Y. P. Chin, The role of fulvic acid composition in the photosensitized degradation of aquatic contaminants, *Aquat. Sci.*, 2009, **71**, 160-169.

10. J. A. Leenheer and J. P. Croué, Characterizing aquatic dissolved organic matter, *Environ. Sci. Technol.*, 2003, **37**, 18A-26A.

11. C. Richard and S. Canonica, in *Handbook of Environmental Chemistry*, ed. O. Hutzinger, Springer-Verlag Berlin, Heidelberger Platz 3, D-14197 Berlin, Germany, 2005, vol. 2, pp. 299-323.

12. J. Hoigné, B. C. Faust, W. R. Haag, F. E. Scully and R. G. Zepp, Aquatic humic substances as sources and sinks of photochemically produced transient reactants, *ACS Sym. Ser.*, 1989, **219**, 363-381.

13. D. Vione, M. Minella, V. Maurino and C. Minero, Indirect photochemistry in sunlit surface waters: photoinduced production of reactive transient species, *Chem. Eur. J.*, 2014, **20**, 10590-10606.

14. J. Wenk and S. Canonica, Phenolic antioxidants inhibit the triplet-induced transformation of anilines and sulfonamide antibiotics in aqueous solution, *Environ. Sci. Technol.*, 2012, **46**, 5455-5462.

15. P. R. Erickson, N. Walpen, J. J. Guerard, S. N. Eustis, J. S. Arey and K. McNeill, Controlling factors in the rates of oxidation of anilines and phenols by triplet methylene blue in aqueous solution, *J. Phys. Chem. A*, 2015, **119**, 3233-3243.

16. R. G. Zepp, P. F. Schlotzhauer and R. M. Sink, Photosensitized transformations involving electronic energy transfer in natural waters - Role of humic substances, *Environ. Sci. Technol.*, 1985, **19**, 74-81.

17. S. G. Cohen, A. Parola and G. H. Parsons, Photoreduction by amines, *Chem. Rev.*, 1973, **73**, 141-161.

18. J. Wenk, U. von Gunten and S. Canonica, Effect of dissolved organic matter on the transformation of contaminants induced by excited triplet states and the hydroxyl radical, *Environ. Sci. Technol.*, 2011, **45**, 1334-1340.

19. J. Wenk, M. Aeschbacher, M. Sander, U. von Gunten and S. Canonica, Photosensitizing and inhibitory effects of ozonated dissolved organic matter on triplet-induced contaminant transformation, *Environ. Sci. Technol.*, 2015, **49**, 8541-8549.

20. F. Leresche, U. von Gunten and S. Canonica, Probing the photosensitizing and inhibitory effects of dissolved organic matter by using *N*,*N*-dimethyl-4-cyanoaniline (DMABN), *Environ. Sci. Tech.*, 2016, **50**, 10997-11007.

21. Z. R. Grabowski, K. Rotkiewicz and W. Rettig, Structural changes accompanying intramolecular electron transfer: Focus on twisted intramolecular charge-transfer states and structures, *Chem. Rev.*, 2003, **103**, 3899-4031.

22. A. Demeter and K. A. Zachariasse, Triplet state dipole moments of aminobenzonitriles, *J. Phys. Chem. A*, 2008, **112**, 1359-1362.

23. W. Rettig, External and internal parameters affecting the dual fluorescence of *p*-cyano-dialkylanilines, *J. Lumines.*, 1981, **26**, 21-46.

24. S. I. Druzhinin, N. P. Ernsting, S. A. Kovalenko, L. W. Lustres, T. A. Senyushkina and K. A. Zachariasse, Dynamics of ultrafast intramolecular charge transfer with 4-(dimethylamino)benzonitrile in acetonitrile, *J. Phys. Chem. A*, 2006, **110**, 2955-2969.

25. J. Catalán, On the dual emission of *p*-dimethylaminobenzonitrile and its photophysical implications, *Phys. Chem. Chem. Phys.*, 2013, **15**, 8811-8820.

26. S. I. Druzhinin, V. A. Galievsky, A. Demeter, S. A. Kovalenko, T. Senyushkina, S. R. Dubbaka, P. Knoche, P. Mayer, C. Grosse, D. Stalke and K. A. Zachariasse, Two-state intramolecular charge transfer (ICT) with 3,5-dimethyl-4(dimethylamino)benzonitrile (MMD) and its meta-isomer mMMD. Ground state amino twist not essential for ICT, *J. Phys. Chem. A*, 2015, **119**, 11820-11836.

27. G. Köhler, G. Grabner and K. Rotkiewicz, Nonradiative deactivation and triplet states in donor aryl acceptor compounds (dialkylaminobenzonitriles), *Chem. Phys.*, 1993, **173**, 275-290.

28. G. Köhler, N. Getoff, K. Rotkiewicz and Z. R. Grabowski, Electron photoejection from donor–aryl-acceptor molecules in aqueous solution, *J. Photochem.*, 1985, **28**, 537-546.

29. G. V. Buxton, C. L. Greenstock, W. P. Helman and A. B. Ross, Critical review of rate constants for reactions of hydrated electrons, hydrogen atoms and hydroxyl radicals ($^{\bullet}OH/^{\bullet}O^{-}$) in aqueous solution, *J. Phys. Chem. Ref. Data*, 1988, **17**, 513-886.

30. R. H. Kayser and R. H. Young, The photoreduction of methylene blue by amines, A flash photolysis study of the reaction between triplet methylene blue and amines, *Photochem. Photobiol.*, 1976, **24**, 395-401.

31. J. C. Ianni, Kintecus Windows version 5.20, 2014. www.kintecus.com (accessed August 2016).

32. F. S. Dainton and D. B. Peterson, Forms of H and OH produced in radiolysis of aqueous systems, *Proc. R. Soc. Lon. Ser-A*, 1962, **267**, 443-463.

33. D. Zehavi and J. Rabani, Pulse radiolytic investigation of Oaq radical ions, *J. Phys. Chem.*, 1971, **75**, 1738-1744.

34. E. Baciocchi, M. Bietti, M. F. Gerini and O. Lanzalunga, Electron-transfer mechanism in the *N*-demethylation of *N*,*N*-dimethylanilines by the phthalimide-*N*-oxyl radical, *J. Org. Chem.*, 2005, **70**, 5144-5149.

35. B. H. J. Bielski, D. E. Cabelli, R. L. Arudi and A. B. Ross, Reactivity of HO_2/O^{-}_2 radicals in aqueous solution, *J. Phys. Chem. Ref. Data*, 1985, **14**, 1041-1100.

36. I. Loeff, J. Rabani, A. Treinin and H. Linschitz, Charge-transfer and reactivity of nπ* and ππ* organic triplets, including anthraquinonesulfonates, in interactions with inorganic anions: A comparative study based on classical Marcus theory, *J. Am. Chem. Soc.*, 1993, **115**, 8933-8942.

37. K. McNeill and S. Canonica, Triplet state dissolved organic matter in aquatic photochemistry: reaction mechanisms, substrate scope, and photophysical properties, *Environ. Sci.: Processes Impacts*, 2016, **18**, 1381-1399.

38. K. Kalyanasundaram, J. Kiwi and M. Gratzel, Hydrogen evolution from water by visible-light, a homogeneous 3 component test system for redox catalysis, *Helv. Chim. Acta*, 1978, **61**, 2720-2730.

39. R. J. Visser, P. C. M. Weisenborn, J. Konijnenberg, B. H. Huizer and C. A. G. O. Varma, Solute solvent exciplexes in the photoinduced formation of radical ions of 4-*N*,*N*-dimethylaminobenzonitrile and related compounds, *J. Photochem.*, 1986, **32**, 217-233.

40. H. Shizuka and H. Obuchi, Anion-induced triplet quenching of aromatic ketones by nanosecond laser photolysis, *J. Phys. Chem.*, 1982, **86**, 1297-1302.

41. D. Rehm and A. Weller, Kinetics and mechanics of electron transfer during fluorescence quenching in acetonitrile, *Ber. Bunsenges. Phys. Chem.*, 1969, **73**, 834-839.

42. D. Rehm and A. Weller, Kinetics of fluorescence quenching by electron and H-atom transfer, *Israel J. Chem.*, 1970, **8**, 259-271.

43. R. A. Marcus, On the theory of oxidation-reduction reactions involving electron transfer .1., *J. Chem. Phys.*, 1956, **24**, 966-978.

44. S. Canonica, B. Hellrung and J. Wirz, Oxidation of phenols by triplet aromatic ketones in aqueous solution, *J. Phys. Chem. A*, 2000, **104**, 1226-1232.

45. M. Jonsson, J. Lind, T. E. Eriksen and G. Merenyi, Redox and acidity properties of 4-substituted aniline radical cations in water, *J. Am. Chem. Soc.*, 1994, **116**, 1423-1427.

46. G. Merényi and J. Lind, in *N-centered radicals*, ed. Z. B. Alfassi, John Wiley & Sons Ltd, Chichester, 1998, ch. 20, pp. 599-613.

47. R. J. Visser and C. A. G. O. Varma, Source of anomalous fluorescence from solutions of 4-*N*,*N*-dimethylaminobenzonitrile in polar solvents, *J. Chem. Soc. Farad. Trans. 2*, 1980, **76**, 453-471.

48. X. M. Zhang, S. R. Yeh, S. Hong, M. Freccero, A. Albini, D. E. Falvey and P. S. Mariano, Dynamics of alpha-CH deprotonation and alpha-desilylation reactions of tertiary amine cation radicals, *J. Am. Chem. Soc.*, 1994, **116**, 4211-4220.

49. G. W. Dombrowski, J. P. Dinnocenzo, P. A. Zielinski, S. Farid, Z. M. Wosinska and I. R. Gould, Efficient unimolecular deprotonation of aniline radical cations, *J. Org. Chem.*, 2005, **70**, 3791-3800.

50. J. M. Burns, W. J. Cooper, J. L. Ferry, D. W. King, B. P. DiMento, K. McNeill, C. J. Miller, W. L. Miller, B. M. Peake, S. A. Rusak, A. L. Rose and T. D. Waite, Methods for reactive oxygen species (ROS) detection in aqueous environments, *Aquat. Sci.*, 2012, **74**, 683-734.